Nanoscale

Accepted Manuscript

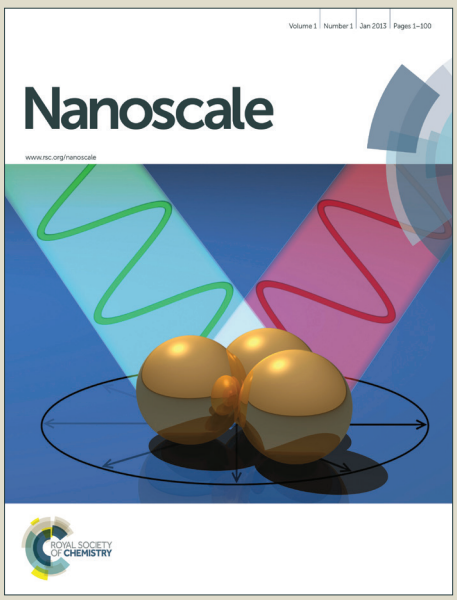

ROYAL SOCIETY OF CHEMISTRY

www.rsc.org/nanoscale

Journal Name

ARTICLE

Received 00th January 20xx,
Accepted 00th January 20xx

DOI: 10.1039/x0xx00000x

www.rsc.org/

Achieving significantly enhanced visible-light photocatalytic efficiency using polyelectrolyte: the composites of exfoliated titania nanosheet, graphene, and poly(diallyl-dimethyl-ammonium chloride)

Qian Zhang,[a] *Qi An,**[a] *Xinglong Luan,*[a] *Hongwei Huang,**[a] *Xiaowei Li,*[a] *Zilin Meng,*[a] *Wangshu Tong,*[a] *Xiaodong Chen,*[b] *Paul K. Chu,*[c] *Yihe Zhang**[a]

A high-performance visible-light-active photocatalyst is prepared using the polyelectrolyte/exfoliated titania nanosheet/graphene oxide (GO) precursor by flocculation followed by calcination. The polyelectrolyte poly(diallyl-dimethyl-ammonium chloride) serves not only as an effective binder to precipitate GO and titania nanosheets, but also boosts the overall performance of the catalyst significantly. Unlike most titania nanosheet – based catalysts reported in the literature, the composite absorbs light in the UV-Vis-NIR range. Its decomposition rate of methylene blue is 98% under visible light. This novel strategy of using a polymer to enhance the catalytic performance of titania nanosheet-based catalysts permits immense potential in designing and fabrication next-generation photocatalysts with high efficiency.

[a] *Beijing Key Laboratory of Materials Utilization of Nonmetallic Minerals and Solid Wastes, National Laboratory of Mineral Materials, School of Materials Science and Technology, China University of Geosciences, Beijing, 100083, P.R. China E-mail: an@cugb.edu.cn; hhw@cugb.edu.cn; zyh@cugb.edu.cn*
[b] *.School of Materials Science and Engineering, Nanyang Technological University, Block N4.1, 50 Nanyang Avenue, Singapore, 639798*
[c] *. Department of Physics & Materials Science, City University of Hong Kong, Tat Chee Avenue, Kowloon, Hong Kong*
[d] *Address here.*
† Electronic Supplementary Information (ESI) available:

Introduction

Visible light constitutes 46% of the solar spectrum and effective utilization of this portion of solar energy can reduce demands for fossil fuels and non-recyclable energy. Visible-light active catalysts that are able to decompose organic pollutants, promote water photolysis, fix CO_2, or selectively oxide organic compounds have thus received tremendous attention [1-4] and in particular titania-based photocatalysts and photovoltaics have been widely studied.[5-7] Although with proper engineering, titania-based catalysts can effectively respond to visible light,[8-12] high-efficiency titania-based visible-light active catalysts are still difficult to produce. In comparison with bulk titania or titania nanoparticles, exfoliated titania nanosheets, which possess the unique two-dimensional (2D) structure, controlled thickness, ample active surface area, abundant hetero-interface, and superior capacity to load sensitizers or substrate molecules, are envisioned to be powerful catalysts.[13,14] Possessing a band gap approximately 0.6 eV larger than that of anatase TiO_2, titania nanosheets have stronger reduction and oxidation power.[13,15] However, titania nanosheets require UV light with even shorter wavelengths for activation due to the larger band gap. To fully realize the redox potential of titania nanosheets that can be activated by visible light, new strategies must be developed. For example, nitrogen doping of titania nanosheets renders them visible-light sensitivity[16] and visible-light-induced H_2 production has been demonstrated from porous assemblies of CdS quantum dot and layered titanate nanosheets.[17] An effective visible-light active photocatalyst suitable for decomposition of organic pollutants prepared by an exfoliation–restacking strategy with chromia nanoparticles and layered titanate has been demonstrated.[18] Furthermore, composite catalysts composed of titania nanosheets, mesoporous silica, and CdS exhibit high hydrogen evolution activity under visible light [19] and assemblies of CdS-titania and iron oxide-titania nanosheets also display effective catalytic ability toward the decomposition of organic pollutants.[20-24] Graphene, an important class of 2D materials, has many favorable optical and electrical properties boasting high flexibility in application and large surface area.[25,26] Graphene has been extensively studied for its possible application to catalysis. For example, robust hollow spheres consisting of titania nanosheets and graphene nanosheets possess strong catalytic activity in the conversion of CO_2 to renewable fuels.[27]

Despite recent technological advances, it is still challenging to fabricate titania nanosheet-based visible-light active photocatalysts. Mostly inorganic materials such as CdS, iron oxide, and chromia nanoparticles can be incorporated

with exfoliated titania nanosheets and nitrogen doping to prepare the catalysts. Compared to anatase TiO_2,[28] the materials employed to engineer titania nanosheets are quite limited and in particular, coupling with organic species has seldom been explored.[29-31] The unique advantages stemming from the structural properties of titania nanosheets remain to be demonstrated and the mechanisms governing the visible-light response compared to those of pristine titania nanosheets or anatase require clarification.

Herein, we report the preparation of a visible-light active photocatalyst using a ternary polyelectrolyte poly(diallyl-dimethyl-ammonium chloride) (PDDA) / graphene oxide (GO) / titania nanosheet precursor and investigate its effectiveness in decomposing methylene blue (MB), a model organic pollutant. Under visible light irradiation, 98% of MB in a 50 ml solution (3×10^{-5} M) is decomposed by only 10 mg of the photocatalyst. The organic polyelectrolyte species (PDDA) not only serves as a binder to precipitate the nanosheets, but also contributes to the overall photocatalytic performance. To the best of our knowledge, this is the first report on the use of an organic polyelectrolyte as an effective component to fabricate titania nanosheet-based composite catalysts.

Results and Discussion

The flexible nanosheets show ample wrinkles as shown by the scanning electron microscopy (SEM) and transmission electron microscopy (TEM) images (Figures 1a-b). The lateral size of the nanosheets is several micrometers and the thickness of the titania sheet is as small as several nanometers. The representative atomic force microscopy (AFM) image with the line scan is shown in Figure 1c. The 1.7 nm shown in the image corresponds to the bilayer thickness.[13] Statistical analysis of the AFM results indicate that more than 52% of the sheets are bilayers having thicknesses between 1 and 2 nm and single-layered nanosheets constitute about 12%. All of the nanosheets are thinner than 5 nm corresponding to less than 5 layers (Figure 1d). XPS and FTIR results indicated that the surfactant $(C4H_9)_4NOH$ presented in the surface of the prepared titania nanosheets (Figure S1&S2). The nanosheets are readily dispersed in water and the transparent suspension displays the Tyndall phenomenon typical of colloids (Figure 1e).

The materials are obtained after flocculation from a mixture of negatively-charged GO (zeta potential of -47.5 mV) and titania nanosheets (zeta potential of -48.5 mV) by positively-charged polyelectrolyte PDDA addition. The precipitate is calcinated in air at 300 °C for 1 h (Scheme 1). PDDA here served double roles as both an effective binder and also a charge-withdrawn agent after calcination as discussed below.[32-34] The zeta potential of the photocatalyst is -52.7 mV. The SEM image of the photocatalyst Figure 2a shows that it is composed of particles with some arbitrary shape and size between several hundred nanometers and several micrometers. The layered structure can be observed from the particles and may arise from the precursor GO or titania nanosheets. The materials have a porous structure with a wide size distribution from several tens of nanometers to as large as a micrometer on the surface. The particles are dominated by C together with O, N, and Ti (Table S1). These elements are distributed evenly throughout the catalyst as indicated by the elemental maps (Figure 2b).

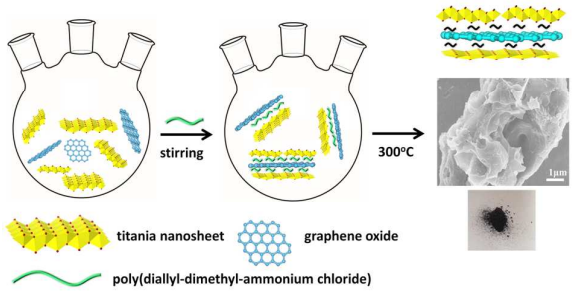

Scheme 1. Schematic illustration of the preparation process of the photocatalyst. PDDA is added to a dispersion comprising GO and titania nanosheets to induce electrostatic aggregation and subsequent calcination at 300 °C produces the photocatalyst.

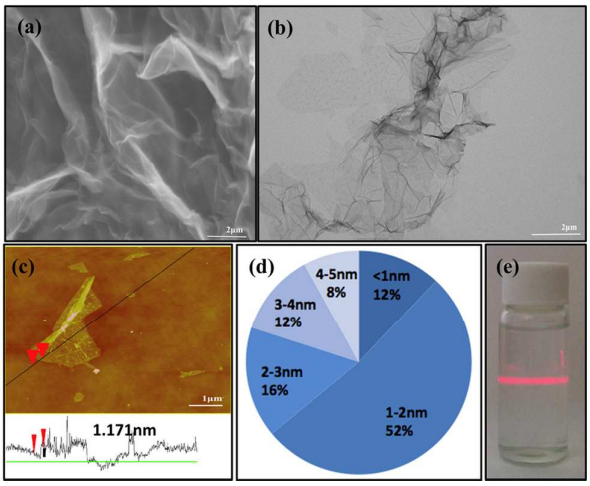

Figure 1. (a) SEM and (b) TEM images of the exfoliated titania nanosh eets. (c) Typical AFM image of the titania nanosheets together with the line scan. (d) Statistical analysis of the titania nanosheet thickness distribution based on AFM performed on 52 pieces. (e) Picture showing the aqueous dispersion of the titania nanosheets showing the Tyndall effect typical of colloids.

The Fourier transform infrared (FTIR) spectra in Figure 3a confirm the elemental composition and indicate that titania, GO, rGO and partially carbonated PDDA co-exist in the catalyst. The existence of PDDA is verified by the doublet of the $-CH_2-$ anti-symmetrical and symmetrical stretching vibration at 2922 cm^{-1} and 2853 cm^{-1}, respectively. The vibration at approximately 1382 cm^{-1} is attributed to $-CH_2-$ alkyl rocking and the C–N stretching vibration at 1152cm^{-1} stems from the amino group in the PDDA. These vibrations indicate the presence of PDDA in the composite in the form of an organic species after calcination. The bands in the range 400-700 cm^{-1} corresponds to the vibrations of the inorganic Ti–O and Ti–O–Ti networks. FTIR also indicates that after calcination,

GO is partially reduced and GO and rGO co-exist in the composite catalyst. The FTIR spectrum of GO in Figure 3a reveals C=O stretching vibration bands at 1716 cm^{-1} and C=C stretching vibration bands of an aromatic ring at 1615 cm^{-1}. The bands at 1051 cm^{-1} and 1211 cm^{-1} are assigned to the C–O symmetrical stretching of C–O–C and C–O stretching of C–OH, respectively. Notably, the stretching bands of the photocatalyst are weaker than those of GO, indicating that after calcination, oxygen-containing functional groups are partially removed from the surface of GO and GO is partly reduced. To investigate the role of PDDA, the FTIR spectra of PDDA and PDDA after calcination were shown in the Figure S3. Comparing with PDDA, the CH_2 symmetric and asymmetric stretching at 2939 cm^{-1} and 3006 cm^{-1} decreased markedly in PDDA-300°C. The vibration at 1382 cm^{-1} attributed to $-CH_2-$ alkyl rocking become weaker. While the C-N stretching at 1109 cm^{-1} still exists. These results indicate the PDDA in the composite were partial carbonized.

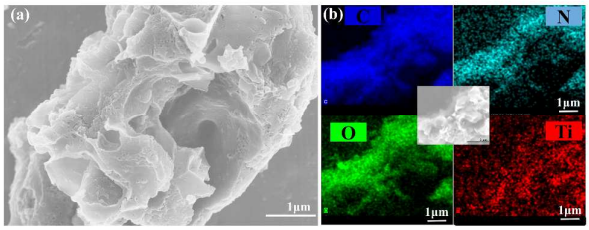

Figure 2. (a) Representative SEM image of the photocatalyst particles. (b) Elemental maps of the photocatalyst showing the distributions of C, N, O and Ti on the photocatalyst particles. An SEM image is displayed in the center of the elemental maps. The scale bars in the images corresponded to 1 μm.

Thermogravimetric analysis (TGA) corroborates that during calcination, GO is reduced and PDDA is carbonized (Figure 3b). The TGA curve of GO measured in air displays three distinct ranges of weight losses as the temperature is increased. The weight loss results from loss of adsorbed water below 120 °C and loss of oxygen-containing functional groups between 120 °C and 300 °C. At a temperature higher than 450 °C, combustion of the GO carbon skeleton occurs.[32] The TGA curve of PDDA also shows three ranges of weight losses with increasing temperature. The weight loss at below 150 °C is again due to the loss of adsorbed water but between 150 °C and 330 °C, the weight of the PDDA does not change. The substantial weight loss observed between 330 °C and 550 °C stems from carbonization of PDDA and the weight loss at >550 °C corresponds to PDDA combustion.[35] Meanwhile, the weight loss of titania sheets in the monitored range is negligible. Compared to the TGA curves for GO and PDDA, the TGA curve of the composite generally resembles that of PDDA, suggesting that the composite is dominated by PDDA. However, characteristic weight losses contributed by GO in the range 150 °C ~ 300 °C and >450 °C are also observable, indicating that during the calcination process at 300 °C, GO is partially reduced, whereas PDDA is already in the carbonization process by considering the delayed effect due to rapid heating to be discussed later. The structure of the catalyst is determined by X-ray powder diffraction (XRD). As shown in Figure 3c, a broad band (2θ) ranging from 20° to 30° dominates the (002) diffraction spectra, indicating the existence of a large amount of amorphous carbon in the catalyst. There are peaks at 32° and 45° at the shoulder of the broad band and they can be indexed to TiO_2 (JCPDS 84-1750). The cell parameters corresponding to this refractive peak were counted by Jade 5.0 as a=4.533 nm, b=5.523 nm, c=4.884 nm, which was close to the cell parameters of TiO_2 (JCPDS 84-1750: a=4.532nm, b=5.502nm, C=4.906nm.) but didn't belong to rutile, anatase, or brookite form.

The photocatalyst absorbs ultraviolet and visible (UV-Vis) light efficiently as shown by the UV-Vis diffuse reflectance spectra (DRS) in Figure 4. The absorbance between 200 and 750 nm is very strong thus encompassing UV-Vis light. The absorbance decreases gradually beyond 750 nm and reaches a horizontal minimum beyond 1400 nm. The catalyst also absorbs near infrared (NIR) light. The materials are thus quite unique being able to absorb light in the V-Vis-NIR range and it is the broadest observed from titania nanosheet-based composites so far.[13,17-24] To probe the origin of the strong and wide absorbance of the photocatalyst, the UV-Vis DRS is compared to those of the single constituents, namely GO, GO calcinated at 300 °C, PDDA, as well as PDDA calcinated at 300°C. As shown in Figure 4, the UV-Vis DRS of the titania nanosheets is within the UV range (200 - 380 nm). GO, whether calcinated or not, absorbs light across the UV-Vis-NIR range. PDDA, without calcination, absorbs light only in the UV range. After calcination at 300 °C for 1 h, the PDDA absorbs light in the UV-Vis-NIR range thereby explaining the strong and

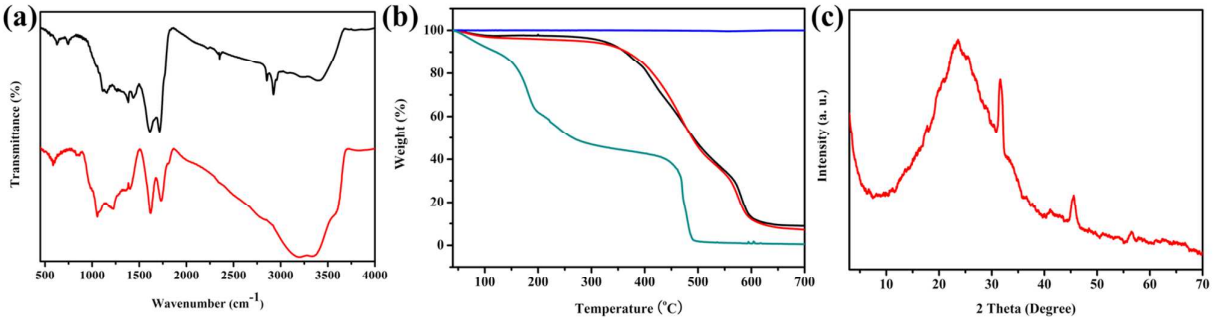

Figure 3. (a) FTIR spectra of the composite catalyst (black) and GO (red). (b) TGA profiles of the catalyst (red), titania sheets (blue), PDDA (black), and GO (green). (c) XRD pattern of the photocatalyst.

wide absorbance profile of the catalyst. Calcinated PDDA, the dominant component in the composite, generates nitrogen-containing carbon and provides strong background absorbance in the UV-Vis-NIR range and the absorbance is enhanced due to the existence of titania nanosheets, GO, and rGO.

species (Figure S4). An identical amount of titania nanosheets only reduces the absorbance of MB by 10% indicating limited capability in the decomposition of MB under visible light. The complex before calcination displayed minimal catalytic power towards the degradation of MB (Figure S5). The degradation

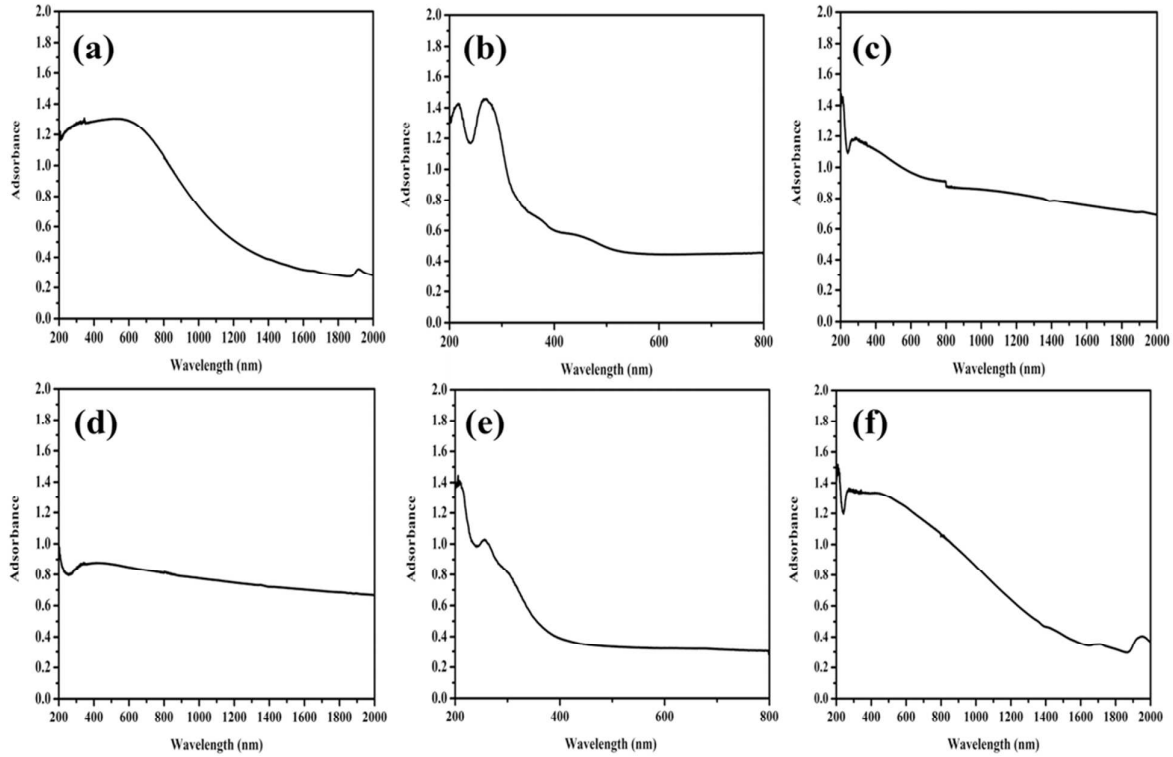

Figure 4. UV-Vis DRS: (a) Composite photocatalyst, (b) Titania nanosheets, (c) GO, (d) GO after calcination at 300 °C, (e) PDDA, and (f) PDDA after calcination at 300 °C.

The photocurrents generated by the composite under visible light irradiation are measured and a strong photocurrent is shown in Figure 5. The photocurrent is generated immediately after turning on the light and reaches a plateau within 10 s. In comparison, the titania sheets before and after calcination and the complex before calcination generate a negligible photocurrent under visible light irradiation (Figure 5). The photocurrent measurements suggest enhanced separation efficiency of the photogenerated carriers in the composite.

The photocatalytic effects under visible light irradiation are determined using MB as the model organic dye. The catalyst (10 mg) was introduced to 50 ml of the MB solution (3×10^{-5} M) and it was maintained in darkness for 30 min to allow adsorption of MB onto the surface of the particles. A short equilibrium period of 30 min was chosen in consideration of the practical application conditions of the catalysts. Afterwards, visible light is turned on to initiate the photocatalytic process (Figure 6). Under optimized conditions, 98% of the MB is removed in 250 min. Accordingly, the total organic content (TOC) of the solution decreases to 22% of the original value indicating effective decomposition of the organic

percentage (98%) is much better than that reported for MB decomposition by titania nanosheet-based catalysts in the literature. ZnO pillared Fe-doped titania nanosheet composite degraded approximately 70% MB (10mg/L) of 100 mL aqueous solution with 40mg samples under visible light irradiation[20]. Cds-pillared titanate composite degraded MB (10mg/L 100ml) by 72.8% under visible light[22]. The compsites of exfoliated titania nanosheets and rGO was reported to present enhanced catalytic power under UV irradiation, but no visible-light catalytic activities were observed.[36] The performance is even superior to that of the previously reported for the P25-graphene composite catalyst (MB decomposition rate of <70% at three times the dosage: 30 mg in 40 ml of MB solution with a comparable concentration) [37] or the P25-carbon nanotube catalyst.[38] To further assess the competitive advantage of our catalyst, a PDDA/P25/GO composite is prepared for comparison. The photocatalytic effect of the catalyst containing P25 is only 10% of that of our photocatalyst prepared with the titania nanosheet precursor (Figure 6).[27] The remarkable elevation of the photocatalytic decomposition rate of MB from 10% for pristine titania nanosheets to 98% for the composite catalyst is appreciable and in order to elucidate the

underlying mechanism, the influence of a series of parameters on the catalytic performance is studied.

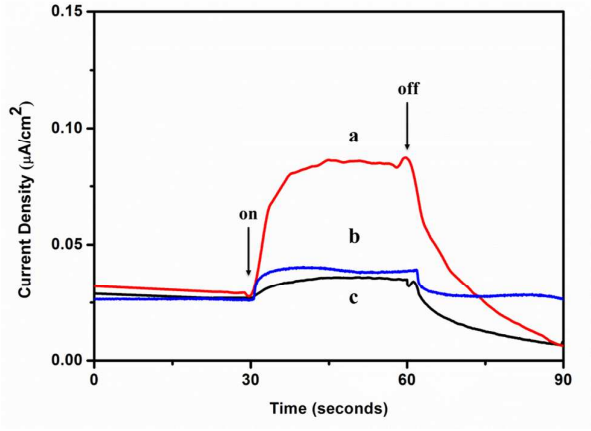

Figure 5. Current generated by (a) composite photocatalyst (b) titania nanosheets after calcinated at 300°C and (c) titania nanosheet under visible light irradiation.

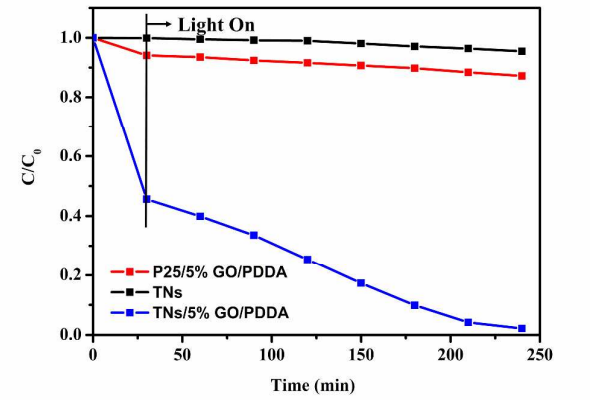

Figure 6. Catalytic performance of titania nanosheets (black). The composite catalyst is prepared with the P25/GO/PDDA precursor (GO fraction of 5%) (red) and titania nanosheet/GO/PDDA precursor (GO fraction of 5%) (blue).

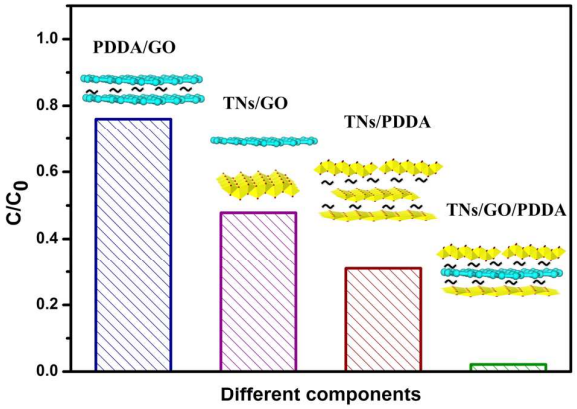

Figure 7. Decrease in MB concentration upon visible light irradiation indicated by decreasing solution absorbance for materials prepared with the titania nanosheets/GO, PDDA/GO, titania nanosheets/PDDA and titania nanosheet/GO/PDDA precursors.

We first examine whether all three components are necessary to obtain the enhanced catalytic performance (Figure 7). Without the titania nanosheets, the absorbance of MB upon irradiation is only approximately 20% of that of the GO/PDDA composite (after calcination) likely due to the adsorption effect.[39] In addition, after PDDA or GO removal, the catalytic performance deteriorates to 50% and 70%, respectively. These results demonstrate all three constituents are necessary to achieve the observed superior catalytic performance.

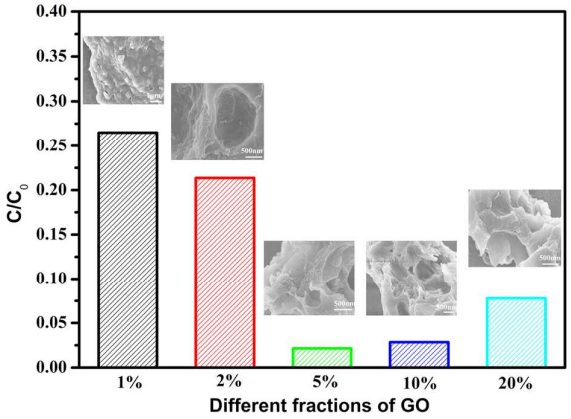

Figure 8. Catalytic performance of the composite photocatalyst prepared with different fractions of GO precursors for decreasing MB concentrations. The SEM images reveal the typical surface morphology of the photocatalysts prepared with different GO precursor fractions of 1%, 2%, 5%, 10%, and 20%.

The influence of the GO fraction is probed to help understand its effect on the catalytic performance. When the GO content is varied from 1% to 20% (percentages denoting the volume percentages of the GO suspension added), the catalytic performance is altered significantly as shown in Figure 8a. The particles prepared with a 5% GO suspension outperform others decomposing 98% of the MB within 250 min. The morphology of the catalysts prepared with different GO fractions is examined by SEM as shown in Figures 2a and 8b-f. Particles with 1% GO show surface bumps but no pores. A GO fraction of 2% leads to a surface morphology with scattered pores with diameters approaching 1 μm. GO fractions of 5% and 10% result in particles with many pores tens to hundreds of nanometers in size. However, when the GO fraction is increased further to 20%, the pores diminish. The surface morphology variations correlate well with the catalytic performance. That is, the catalysts with the best performance (GO fractions of 5% and 10%) have many pores. The BET measurement indicate that the surface area of the particles is only 2.5 $m^2 g^{-1}$, which is substantially smaller than that of mesoporous particles, suggesting that only there are macropores in large quantities but there is no mesoporous structure. The results also indicate that GO is indispensable in obtaining the advanced catalytic performance and the porous structure enhances the performance by increasing the surface for MB adsorption and subsequent decomposition.

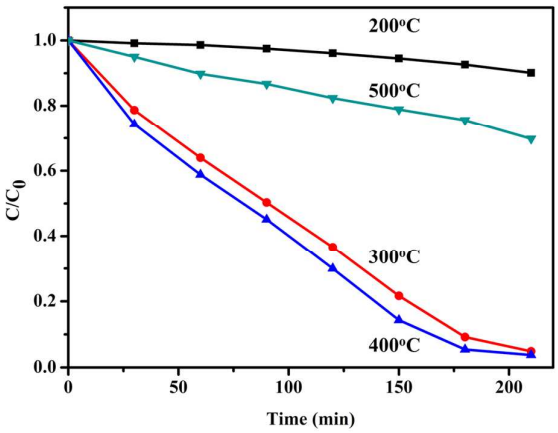

Figure 9. Catalytic performance of catalysts calcinated at different temperatures for decreasing MB concentrations.

The influence of the calcination temperature is evaluated (Figure 9). The particles calcinated at 400 °C for 1 h exhibit the optimal catalytic effect and those calcinated at 300 °C deliver a comparable, albeit slightly inferior, performance. Particles calcinated at 200 °C or 500 °C show worse catalytic effects with the absorbance of MB decreasing by only 8% and 29%, respectively. In conjunction with TGA, it can be concluded that calcination at 300 °C or 400 °C partially reduces GO and carbonates PDDA. Although carbonation of PDDA starts at approximately 330 °C, considering the delay in the onset of the carbonation temperature in the TGA rapid heating process, it is reasonable to assume that PDDA carbonation already occurs at 300 °C. It is supported by the enhanced absorbance of PDDA after calcination (Figure 4). During calcination at 200 °C, reduction of GO occurs but not carbonation of PDDA. The substantially worse catalytic performance after calcination at 200 °C demonstrates that PDDA carbonation is necessary. After calcination at 500 °C, all the PDDA has carbonized and GO is completely consumed. The inferior catalytic performance of the composite calcinated at 500 °C demonstrates that rGO is also necessary for the enhanced catalytic performance. According to previous studies, rGO is a good electronic conductor transferring the generated electrons to the titania nanosheets where the active catalytic centers are generated.[40-43]

The role of PDDA is investigated. After partial carbonization, PDDA generates nitrogen-containing carbon leading to enhanced catalytic performance.[44-45] It is thus interesting to find out whether other polymers can serve as carbon and nitrogen precursors to enhance the catalytic performance. Polyethylenimine (PEI) and poly(allylamine hydrochloride) (PAH) are nitrogen-containing polyelectrolytes [27,46] used to replace PDDA and the catalytic ability is evaluated. As shown in Figure 10, the performances of the new composite are worse than that of the calcinated PDDA / titanianosheets / rGO ternary composite, but better than that of the calcinated titania nanosheets / rGO binary composite (Figure 7). The results indicate that other polymeric precursors that generate nitrogen-doped carbon during calcination can alter the catalytic properties but the performance is inferior to that observed from the materials prepared with the PDDA precursor. It may be explained by that PDDA possesses the electron-withdrawing ability thus creating delocalized net-positive charges on graphene to alter the electronic properties.[32,47] Surface modification of 2D inorganic nanosheets by organic species may alter the intrinsic physical properties leading to different catalytic performance[48] and more work is needed to unravel the exact mechanism. All in all, our results reveal that in order to achieve the best catalytic capability, all three components, namely rGO, carbonated PDDA, and titania nanosheets are necessary. During light irradiation, electrons generated from the carbonated PDDA and rGO migrate to and are injected into the titania nanosheet CB to take part in the redox reactions.[43] Additionally, the porous structure is also crucial to the catalytic performance.

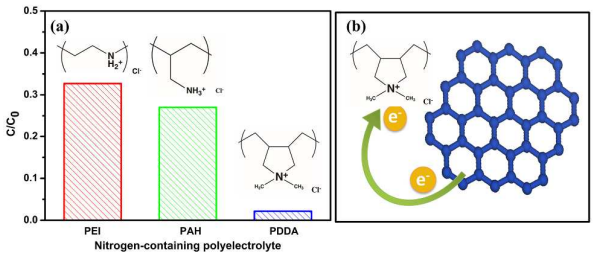

Figure 10. (a) Catalytic performance of the composite catalyst prepared with the PEI/GO/titania nanosheets, PAH/GO/titania nanosheets and PDDA/GO/titania nanosheets precursors for decreasing MB concentrations. (b) Schematic illustration of the electron transfer from graphene to PDDA.

Conclusions

A visible-light photo catalyst comprising GO, PDDA, and titania nanosheets are prepared. The materials exhibit an MB decomposition efficiency of 98% within 250 min under visible light irradiation and the performance is among the best reported for titania-based catalysts. The influence of various parameters and mechanism are investigated. The proper combination of partially carbonated PDDA, reduced GO, and titania nanosheets enables efficient absorption of visible light resulting in enhanced photocurrents and superior photocatalytic performance that is better than that observed from P25-graphene. By adopting the novel strategy of using organic species, the catalytic performance of titania nanosheet-based photocatalyst can be enhanced significantly.

Experimental

Preparation of photocatalyst

The photocatalyst was prepared by slow addition of graphene oxide nanosheets to titania nanosheets under stirring at room temperature for one hour in 25ml beaker. The aqueous PDDA solution was then added slowly to the suspension and stirred for 1 hour to produce the precipitate which was subsequently annealed at 300 °C for 1 hour. The concentrations of titania

nanosheets and GO in the suspension were 0.08 g L^{-1} and 0.1 g L^{-1}, respectively, and that of the PDDA solution was 20 g L^{-1} with a pH of 9. The volume ratio of the GO suspension to titania suspension was 5%. The added volume of PDDA solution was 5 ml. In the experiments to investigate the influence of the parameters, the fraction of GO was varied as described in this paper.

Photocatalytic activity

The photocatalytic activity of the samples was monitored by the degradation of MB in the aqueous solution exposed to visible light from a Xe lamp with an average intensity of 14.6 mW cm^{-3}. A cut-off filter was equipped with the light source (λ > 400 nm). The photocatalyst (10 mg) was dispersed in 50 ml of the dye solution (3×10^{-5} M). Before light illumination, the photocatalyst and dye solution were vigorously stirred in darkness for 0.5 h to achieve the adsorption-desorption equilibrium. After light exposure, 3 mL of the suspension was taken out at certain intervals and the MB concentration was determined at 665 nm by UV-vis measurements after centrifugation.

Acknowledgements

This work was supported by the NSFC (21303169), Fundamental Research Funds for the Central Universities (2652013115), Beijing Nova Program (Z141103001814064), Beijing Specific Project to Foster Elitist (2013D009015000001), Open Project of State Key Laboratory of Chemical Resource Engineering (CRE-2013-C-201), National High Technology Research and Development Program of China (863 Program 2012AA06A109), special co-construction project of Beijing city education committee, and City University of Hong Kong Strategic Research Grant (SRG) No. 7004188.

Notes and references

1 D. M. Schultz, T. P. Yoon, *Science*. 2014, 343, 1239176.
2 Z. Han, F. Qiu, R. Eisenberg, P. L. Holland, T. D. Krauss, *Science* 2012, 338, 1321.
3 J. Luo, J. H. Im, M. T. Mayer, M. Schreier, M. K. Nazeeruddin, N. G. Park, S. D. Tilley, H. J. Fan, M. Grätzel, *Science* 2014, 345, 1593.
4 X. Lang, X. Chen, J. Zhao, *Chem. Soc. Rev.* 2014, 43, 473.
5 H. Lin, Z. Wu, Y. Jia, W. Li, R. K. Zheng, H. Luo, *Appl. Phys. Lett.* 2014, 104, 162907.
6 L. Liang, Y. Liu, C. Bu, K. Guo, W. Sun, N. Huang, T. Peng, B. Sebo, M. Pan, W. Liu, S. Guo, X. Z. Zhao, *Adv. Mater.* 2013, 25, 2174.
7 W. Guo, C. Xu, X. Wang, S. Wang, C. Pan, C. Lin, Z. L. Wang, *J. Am. Chem. Soc.* 2012, 134, 4437.
8 X. Lang, W. R. Leow, J. Zhao, X. Chen, *Chem. Sci.* 2015, 6, doi: 10.1039/ C4SC02891K.
9 R. Asahi, T. Morikawa, T. Ohwaki, K. Aoki, Y. Taga, *Science* 2001, 293, 269.
10 X. Chen, A. Selloni, *Chem. Rev.* 2014, 114, 9281.
11 J. Schneider, M. Matsuoka, M. Takeuchi, J. Zhang, Y. Horiuchi, M. Anpo, D. W. Bahnemann, *Chem. Rev.* 2014, 114, 9919.
12 R. Asahi, T. Morikawa, H. Irie, T. Ohwaki, *Chem. Rev.* 2014, 114, 9824.
13 L. Wang, T. Sasaki, *Chem. Rev.* 2014, 114, 9455.
14 M. Osada, T. Sasaki, *J. Mater. Chem.* 2009, 19, 2503.
15 H. Sato, K. Ono, T. Sasaki, A. Yamagishi, *J. Phys. Chem. B* 2003, 107, 9824.
16 G. Liu, L. Wang, C. Sun, Z. Chen, X. Yan, L. Cheng, H. Cheng, G. Q. M. Lu, *Chem. Commun.* 2009, 11, 1383.
17 H. N. Kim, T. W. Kim, I. Y. Kim, S. J. Hwang, *Adv. Funct. Mater.* 2011, 21, 3111.
18 T. W. Kim, S. G. Hur, S. J. Hwang, H. Park, W. Choi, J. H. Choy, *Adv. Funct. Mater.* 2007, 17, 307.
19 J. Zhang, Z. Zhu, Y. Tang, K. Müllen, X. Feng, *Adv. Mater.* 2014, 26, 734.
20 K. Z. Zhang, B. Z. Lin, Y. L. Chen, B. H. Xu, X. T. Pian, J. D. Kuang, B. Li, *J. Colloid Interf. Sci.* 2011, 358, 360.
21 B. Li, B. Z. Lin, O. Zhang, L. M. Fu, H. Liu, Y. L. Chen, B. F. Gao, *J. Colloid Interf. Sci.* 2012, 386, 1.
22 J. Fu, G. Li, F. Xi, X. Dong, *Chem. Eng. J.* 2012, 180, 330.
23 X. Yan, G. Liu, L. Wang, Y. Wang, X. Zhu, J. Zou, M. Qing, G. Lu, *J. Mater. Res.* 2010, 25, 182.
24 T. W. Kim, H. W. Ha, M. J. Paek, S. H. Hyun, I. H. Baek, J. H. Choy, S. J. Hwang, *J. Phys. Chem. C* 2008, 112, 14853-14862.
25 A. K. Geim, *Science* 2009, 324, 1530.
26 H. Y. Mao, S. Laurent, W. Chen, O. Akhavan, M. Imani, A. A. Ashkarran, M. Mahmoudi, *Chem. Rev.* 2013,113, 3407.
27 W. Tu, Y. Zhou, Q. Liu, Z. Tian, J. Gao, X. Chen, H. Zhang, J. Liu, Z. Zou, *Adv. Funct. Mater.* 2012, 22, 1215.
28 M. Dahl, Y. Liu, Y. Yin, *Chem. Rev.* 2014, 114, 9853.
29 T. Yamamoto, N. Saso, Y. Umemura, Y. Einaga, *J. Am. Chem. Soc.* 2009, 131, 13196.
30 Y. Umemura, E. Shinohara, A. Koura, T. Nishioka, T. Sasaki, *Langmuir* 2006, 22, 3870.
31 T. Sasaki, Y. Ebina, K. Fukuda, T. Tanaka, M. Harada, M. Watanabe, *Chem. Mater.* 2002, 14, 3524.
32 S. Wang, D. Yu, L. Dai, D. W. Chang, J. B. Baek, *ACS Nano* 2011, 5, 6202.
33 M. Cheng, F. Shi, J. Li, Z. Lin, C. Jiang, M. Xiao, L. Zhang, W. Yang, T. Nishi. Adv. Mater. 2014, 26, 3009.
34 Y. Li, P.Cui, L. Wang, H. Lee, K. Lee, H. Lee. ACS Appl. Mater. Interfaces 2013, 5, 9155.
35 J. Zhang, J. Jiang, X. S. Zhao, *J. Phys. Chem. C* 2011, 115, 6448.
36 X. Luan, M. T. G. Wing, Y. Wang, Mat. Sci. Semicon. Proc. 2015, 30, 592.
37 H. Zhang, X. Lv, Y. Li, Y. Wang, J. Li, *ACS Nano* 2009, 4, 380.
38 Y. Zhang, Z. R. Tang, X. Fu, Y. J. Xu, *ACS Nano* 2010, 4, 7303.
39 C. A. Tao, J. Wang, S. Qin, Y. Lv, Y. Long, H. Zhu, Z. Jiang, *J. Mater. Chem.* 2012, 22, 24856.
40 K. K. Manga, Y. Zhou, Y. Yan, K. P. Loh, *Adv. Funct. Mater.* 2009, 19, 3638.
41 M. Long, Y. Qin, C. Chen, X. Guo, B. Tan, W. Cai, *J. Phys. Chem. C* 2013, 117, 16734.
42 Y. T. Liang, B. K. Vijayan, O. Lyandres, K. A. Gray, M. C. Hersam, *J. Phys. Chem. Lett.* 2012, 3, 1760.
43 X. Bai, L. Wang, Y. Zhu, *ACS Catal.* 2012, 2, 2769.
44 Y. Shao, J. Sui, G. Yin, Y. Gao, *Appl. Catal. B-Environ.* 2008, 79, 89.
45 W. Shen, W. Fan, *J. Mater. Chem. A* 2013, 1, 999.
46 Y. Zhou, M. Cheng, X. Zhu, Y. Zhang, Q. An, F. Shi, *ACS Appl. Mater. Inter.* 2013, 5, 8308.
47 S. Wang, D. Yu, L. Dai, *J. Am. Chem. Soc.* 2011, 133, 5182.
48 Y. Guo, K. Xu, C. Wu, J. Zhao, Y. Xie, *Chem. Soc. Rev.* 2015, 44, 637.